Effect of annealing temperature on SnS thin films for photodetector applications

Devarajan Alagarasan[1],* [ORCID], S. S. Hegde[2], S. Varadharajaperumal[3], K. Deva Arun Kumar[4], R. Naik[5], Sathiya Priya Panjalingam[1], Ehab El Sayed Massoud[6,7,8], and R. Ganesan[1],*

[1] Department of Physics, Indian Institute of Science, Bangalore 560012, India

[2] Department of Physics, CMR Institute of Technology, Bengaluru 560037, India

[3] Centre for Nano Science and Engineering, Indian Institute of Science, Bangalore 560012, India

[4] PG & Research Department of Physics, Arul Anandar College, Karumathu, Madurai, Tamil Nadu 625514, India

[5] Department of Engineering and Materials Physics, Institute of Chemical Technology-Indian Oil Odisha Campus, Bhubaneswar 751013, India

[6] Biology Department, Faculty of Science and Arts in Dahran Aljnoub, King Khalid University, Abha, Saudi Arabia

[7] Research Center for Advanced Materials Science (RCAMS), King Khalid University, Abha, Saudi Arabia

[8] Agriculture Research Centre, Soil, Water and Environment Research Institute, Giza, Egypt

ABSTRACT

Tin sulfide (SnS) thin films were deposited at room temperature (RT) by thermal evaporation method and subsequently annealed at 150–350 °C in N_2 atmosphere. The influence of annealing temperature on composition, structural, morphological and optical properties of the thin films has been investigated. X-ray diffraction (XRD) analysis and Raman studies confirmed the formation of single phase SnS films at RT and annealed up to 300 °C. The crystallite size increased from 24 nm for as-deposited film to 37 nm for the 300 °C annealed film and further reduced to 18 nm for the 350 °C annealed film. The film annealed at 200 °C was found to have better morphological features with (111) preferred oriented crystallites. The absorption coefficient, optical band gap (E_g) of the deposited films were estimated from the optical transmittance measurements. Photodetectors are fabricated by depositing Ag contacts on SnS thin films using a metal mask and photo response was tested under dark and illumination conditions using 532 nm laser of varying power intensities. The photodetectors performance is evaluated using responsivity (R), external quantum efficiency (EQE), and specific detectivity (D^*). The specific detectivity of 6.8×10^{10} Jones obtained in the present study is nearly two orders of magnitude greater than that reported earlier.

Address correspondence to E-mail: alagarasanph@gmail.com; rajamanickam.ganesan@gmail.com

1 Introduction

Two-dimensional layered semiconductors such as metal chalcogenides have garnered considerable interest due to their prospective use applications in photovoltaics, visible and NIR detectors, field effect transistors, visible light-induced photocatalysis, thermoelectric [1–4]. Dittrich et al. [5] compiled potential application of sulfo salts in energy conversion, phase change memory, X-ray detectors and cryo-electronics. Semiconducting layered transition-metal chalcogenides (TMDCs) such as MoS_2, $MoSe_2$, WS_2, WSe_2, In_2S_3, CdS: Al and SnS_2 materials possess favorable optical and electrical properties and have been investigated for photodetector applications [6, 7].

In recent years, tin chalcogenides viz., SnS, SnS_2 has gained significant importance for photovoltaic and photodetector applications due to their favorable optical and electrical properties [8, 9]. These semiconducting materials are made up of inexpensive, non-toxic and earth-abundant constituents. Tin sulfide (SnS) possess a direct optical band gap of $\sim$ 1.3 eV and higher coefficient of absorption ($> 10^4$ cm^{-1}) in the visible region. It is used in variety of applications, including solar cells [10], photodetectors [11] gas sensors [12] and as anode materials in Li-ion and Na-ion batteries [13]. Solar cells have been fabricated with SnS as absorber layer with highest efficiency of 4.8%. Tin sulfide intrinsically is a p-type semiconductor and its electrical properties can be easily altered by doping with In, Sb, Ag, Cu etc., [14]. In addition, some findings reported like SnS and SnS_2 are better alternate to silicon and CdS for optoelectronic applications.

Sinsermsuksakul, et.al The SnS band gap value ($\sim$ 1.1 eV) is same to silicon value, but the SnS optical absorption coefficient value is higher than silicon. Silicon material cost is too high. So, SnS would be a very good alternate material of silicon in future [15]. Javed et al. revealed SnS band gap value defined around 1.30 eV in room temperature and it is having higher absorption coefficient ($\alpha \sim 10^4$–10^5 cm^{-1}) in the solar spectrum, the band gap value showing in the region of silicon (1.12 eV) and GaAs (1.43 eV). This SnS is suitable material for photovoltaic device as an absorbing layer and NIR detectors [16]. Maryam et al. reported SnS_2 is anticipated as a proper and alternate buffer to the conventional CdS. Furthermore, the SnS_2 optical properties like absorption coefficient and conduction band offset of 0.21 eV and 0.28 eV results almost unique to CdS [17]. Ullah, et.al, discussed due to flexible band gap (2.2–2.4 eV) behaviour of SnS_2 can be replace the buffer layer of CdS [18]. Xu, et al., reported SnS is a one of the IV–VI semiconductor nanoparticles such as PbS, PbSe, SnTe and GeS, These are optically active materials from NIR to IR region, so lots of scopes are there in the field photovoltaics, near-infrared detectors, and biomedical applications [19].

Previously conducted research on SnS single crystal indicated the presence of a broad absorption band in the visible and near-infrared ranges ($\sim$ 400–1000 nm) of the spectrum [20]. Recently, a polymorph of SnS having cubic crystal structure and direct band gap of 1.7 eV has been identified and it has attracted great attention of researchers owing to its optical band gap, high absorption coefficient and thermal stability [21]. Thin films of SnS were prepared using various thin film fabrication techniques like sputtering, atomic layer deposition, sol–gel, chemical bath deposition, thermal evaporation, spray pyrolysis, etc. [22, 23]. Among these, thermal evaporation method offers better deposition rate, highly purity films with low cost and lesser complexity in material synthesis which is better suited for photo detector applications.

Research on SnS films largely focused on characterization and optimization of the physical properties and its application in photovoltaics. However, there has been little attention on the photo-response characteristics [24]. There are quite a few reports on fabrication of SnS based thin film photodetector and its characterization. Reddy et al. [25] reported the photo response parameters of SnS thin film of varied thickness deposited by co-evaporation technique at 300 °C. It was found that the photoconductivity, photoresponsivity, specific detectivity of the films were increased with increase of film thickness and the obtained maximum responsivity of 0.43×10^{-3} A W^{-1} for the film of 915 nm thickness. Mahdi et al. [26] reported flexible SnS photodetector on a polyethylene terephthalate (PET) substrate by chemical bath method and observed the maximum sensitivity (I_{light}/I_{dark} ratio) of 1604 for 530 nm wavelength at 5 V bias voltage. Liu et al. [27] have studied the 2D nanoflakes of SnS via CVD method and demonstrated high responsivity of 156 AW^{-1} and fast response time of 5.1 ms under illumination of 405 nm laser. Jethwa et al. [28] observed responsivity of

2.16×10^{-2} mAW^{-1} for SnS single crystals under zero biasing voltage and illumination of 670 nm laser.

There are some reports on high-performance photo detector fabricated using SnS nano-structures like nanoflakes [29], nano-belts [30]. Tin sulfide (SnS) is also investigated for NIR photodetector application due to its broad absorption range of light photons [31]. Mahdi et al. [32] assessed suitability of cubic SnS to fabricate high performance broad band UV to NIR photodetector. The photoresponse of SnS-based devices in various gas conditions revealed that photosensitivity is increased in O_2 (or air) compared to vacuum [33]. The effect of annealing on several photodetection parameters such as efficiency, responsivity, and detectivity of SnS films formed via thermal evaporation is not documented. To the best of our knowledge, our work demonstrates the highest responsivity value (0.06 AW^{-1}), highest external quantum efficiency (EQE) value of 14%, and the highest detectivity value of 6.8×10^{10} jones for a 200 °C annealed visible light detector device.

In the current work, SnS thin films were prepared on glass substrates at the optimized conditions under room temperature. The as-deposited samples were annealed in N_2 atmosphere at different temperature in the range of 150–350 °C to enhance its crystallinity and optimize their property for visible light photodetector application.

2 Experimental and characterization techniques

SnS synthesized through the melt-quenching process using high-purity (99.99%) elements Sn and S contained in a quartz ampoule sealed at a pressure of 10^{-5} Torr. To avoid pressure buildup and cracking of the ampoule, the furnace temperature was gradually increased to 600 °C at a rate of 2 °C/min and sustained for 24 h. Although SnS has a melting point of 882 °C, the interaction between Sn and S begins at approximately 600 °C [34]. The furnace temperature was increased to 900 °C, held for 12 h, and then gradually cooled to room temperature.

Thermal evaporation was used to develop SnS thin films under high vacuum (10^{-6} Torr) while maintaining the substrate at ambient temperature. The substrates were ultrasonically cleaned glass slides. The evaporation rate was set at 5 Å/s and the distance between source and substrate was kept at

15 cm, respectively. The as-deposited films were vacuum annealed for 2 h at temperatures ranging from 150 to 350 °C (at intervals of 50 °C).

FESEM (Carl Zeiss Ultra 55) instrument is employed to determine the topographical view and thickness of the prepared thin films. The elemental composition of the films was investigated using the (Oxford Instruments 50 mm^2 instrument). The thin films structural properties were identified using an X-ray diffractometer (Rigaku MiniFlex 600) and Raman spectroscopy. At room temperature, the optical properties of the prepared samples in the spectral region 200 nm–1100 nm were determined using a UV–Vis spectrometer (SpectraPro2300i). The photosensing responses of all the fabricated detectors were obtained using a laser light source of wavelength 532 nm and a Keithley 2450 source meter.

3 Results and discussion

The as-developed and thin films annealed were well adherent to the substrate and pin-hole free.

The adhesion of the films increased when the annealing temperature was increased. A hot-probe test revealed that all thin films possess p-type conductivity.

3.1 Composition and surface morphology

The EDS analysis confirms that the as-deposited and SnS thin films annealed are nearly stoichiometric except for the film annealed at 350 °C. The details of the atomic percent of Sn and S at various annealing temperatures are presented in Table 1. The result revealed that the stoichiometric of SnS can be obtained even at room temperature (RT). This is in contrast to a previously reported work in which

Table 1 Composition of SnS thin film prepared at RT and the films annealed at various temperatures in N_2 atmosphere

Annealing temperature (°C)	Sn (at.%)	S (at.%)	Sn/S (at.%)
As-deposited at RT	50.46	49.54	1.01
150 °C	49.85	50.15	0.99
200 °C	50.02	49.98	1.00
250 °C	49.48	50.52	0.98
300 °C	50.55	49.45	1.02
350 °C	50.65	49.35	1.03

sulfur-rich SnS films produced at lower substrate temperatures (50–100 °C) were found to contain impurity phases SnS_2 and Sn_2S_3 [34]. The sulfur deficiency observed at the films annealed at 350 °C could be attributed to S re-evaporation from the thin films surface due to its high vapor pressure.

Figure 1 portrays the FE-SEM micrographs of the as-deposited SnS film and the films annealed at 200 °C, 300 °C and 350 °C. The films deposited at room temperature shows uniformly distributed rice grain structure morphology with distinctly visible amorphous background. With increase in annealing temperature, amorphous background disappears and the film annealed at 200 °C shows densely packed well grown grains due to re-crystallization process. In the process of re-crystallization, re-orientation of the crystallites within the grain continues up to 300 °C due to maintaining the required thermal energy for the surface diffusion. However, 350 °C annealed film shows quite a few smaller grains presumably due to fragmentation of large grains and presence of other impurity phases of SnS_2. These results are consistent with the observed XRD pattern for the annealed films. Cross sectional view of SEM images showed the reduction of films thickness for higher annealing temperature at 350 °C. This might be due to the

presence of impurity phase of SnS_2 which is confirmed in the XRD and Raman results.

3.2 X-ray diffraction and Raman studies

Figure 2 shows the XRD patterns of the as-deposited and SnS thin films annealed at different temperatures i.e. 150 to 350 °C. The films were phase identified by comparing their measured d-spacing values to those in standard JCPDS files for the respective compounds, namely SnS (JCPDS file no. 39-0354), SnS_2 (JCPDS file no. 23-0677) and Sn_2S_3 (JCPDS file no. 14-0619). All diffraction peaks seen in the as-deposited film were orthorhombic crystal structures of SnS, and no other impurity phases were observed in the XRD pattern. The degree of crystallinity increased with annealing temperature up to 300 °C and further decreased for higher temperature at 350 °C. At 200 °C, degree of preferred orientation (DPO) of (111) diffraction peak was maximum due to oriented crystallites in the film. As the annealing temperature increased to 350 °C, the intensity of (111) diffraction peak gradually decreased due to the origin of impurity phase of SnS_2 become the dominant ones. It is demonstrated that the growth and annealing temperature plays a crucial role in determining the phase and purity of the SnS films. Crystallite size increased to 37 nm for the film annealed at 300 °C from 24 nm

**Fig. 1** FE-SEM images of as-deposited and different annealing temperature (Inset, the cross-sectional image of the same film)
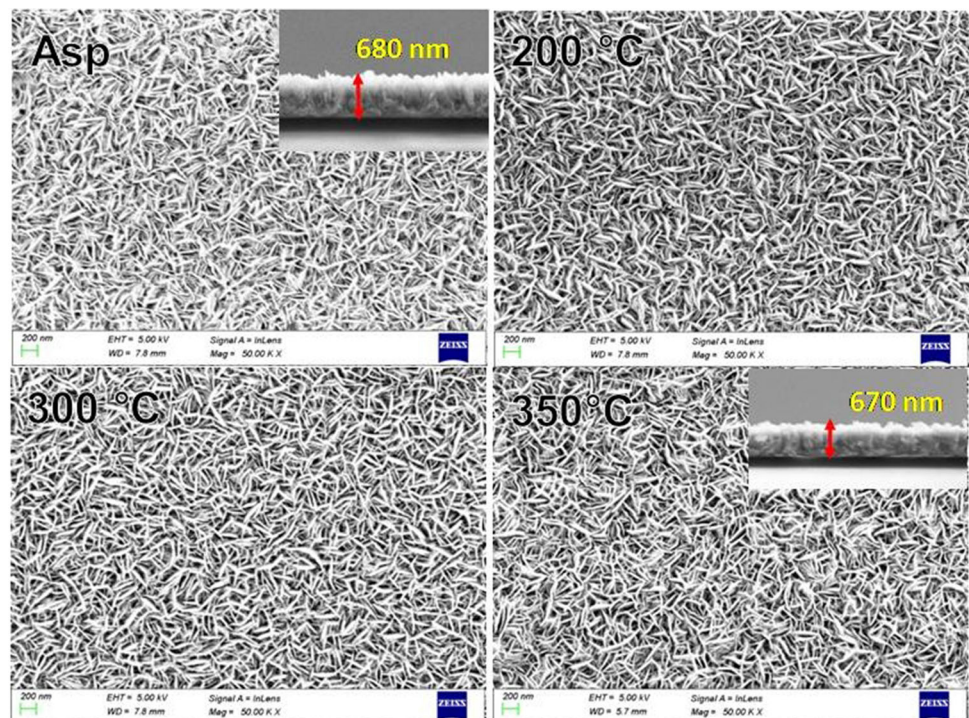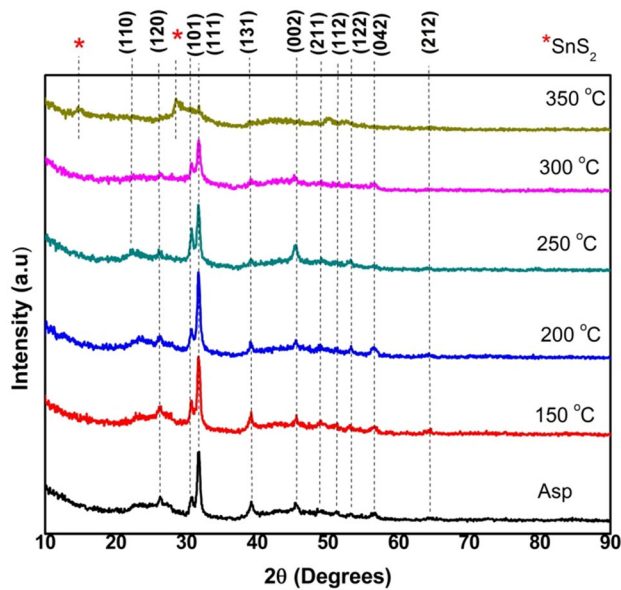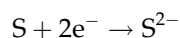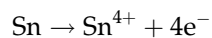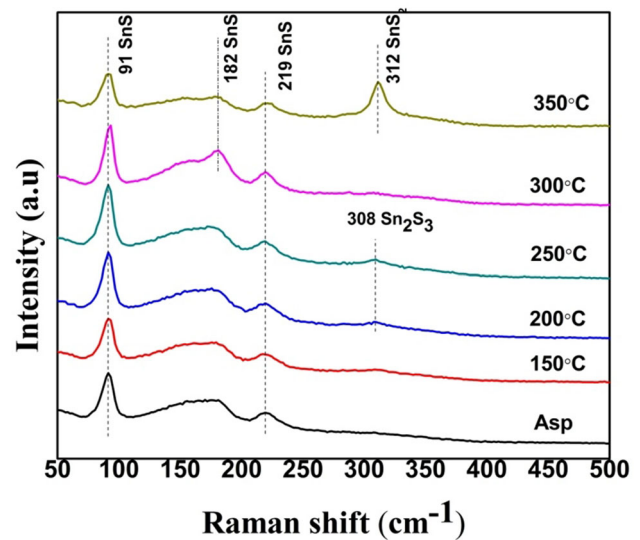
Fig. 2 XRD patterns of as-deposited SnS thin film at RT and films annealed at different temperature in N_2 atmosphere.

Fig. 3 Raman spectra of as-deposited and different annealed SnS thin films

(for as-deposited) and further reduced to 18 nm for the film annealed at 350 °C.

Hegde et al. [35] reported the increase in the crystallite size for the thermally evaporated films at high-substrate temperature of 300 °C and subsequently vacuum annealed. The increase in crystallite size with annealing temperature is also dependent on the film thickness and is impeded for thicker film as reported by Jain et al. [36]. Annealing at 200 °C or higher temperatures is required for re-crystallization, which may result in an increase in the size of the crystallites. Smaller crystals on the substrate absorb heat energy and coalesce or fuse together to form larger crystallites. The observed enlargement of crystallite size is consistent with the reported values in literature [36]. The formation of SnS_2 phases at an annealing temperature of 350 °C may arise in the following way;

$$Sn \rightarrow Sn^{4+} + 4e^-$$

$$S + 2e^- \rightarrow S^{2-}$$

$$Sn^{4+} + 2S^{2-} \rightarrow SnS_2$$
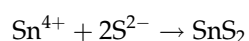
Raman spectroscopy is an effective technique used in identification of the different phases in the prepared samples. Figure 3 shows the Raman spectra of as-deposited and annealed SnS thin films at different temperature ranging from 150 to 350 °C. In

orthorhombic SnS with 8 atoms per unit cell, 24 normal vibration modes as follows:

$$T = 4A_g + 2B_{1g} + 4B_{2g} + 2B_{3g} + 2A_u + 4B_{1u} + 2B_{2u} + 4B_{3u}$$

where, $4A_g$, $2B_{1g}$, $4B_{2g}$ and $2B_{3g}$ are Raman active [21]. The Raman spectrum of as-deposited and SnS thin films annealed exhibits 3 distinguished Raman modes of orthorhombic SnS at 91 cm^{-1} (A_g), 182 cm^{-1} (A_g), 219 cm^{-1} (Ag). The characteristic peaks from the other secondary phases such as Sn_2S_3 and SnS_2 wasnot observed in as-deposited SnS film indicating the formation of pure SnS phase. A weak Raman peak observed at 308 cm^{-1} for thin films annealed at 200 °C and 250 °C might be associated with Sn_2S_3 mode. Mahdi et al. [26] observed the same Sn_2S_3 phase with the preparartion of SnS thin films through chemical bath deposition (CBD). However, the deposited SnS films have strong SnS phase when compared to the Sn_2S_3. Further, the Sn_2S_3 peak was completely disappeared when the film was annealed at 300 °C. Meanwhile, SnS_2 is detected in the film annealed at 350 °C due to their characteristic Raman peaks at 312 cm^{-1}; this may be due to the intralayer vibration of chalcogen–chalcogen process. In addition to that the peak intensity of SnS reduced significantly and the major component turns over to be SnS_2 phase, which agrees well with the abovementioned XRD results.

3.3 Optical properties

Figure 4a shows the transmittance spectra of all the prepared SnS films at different temperatures ranging from 150 to 350 °C. The spectra exhibit transmission in longer wavelength region, since no appropriate electronic transitions are possible. Also, pronounced interference fringes are observed in the transmittance response due to the overlapping of light reflected on both sides of the thin film and it confirms the uniformity in the films thickness [37]. Due to the commencement of fundamental absorption, the reported transmittance drops rapidly near the visible area. All the films show high absorption in the visible region indicating suitability of thin films of SnS (thickness ~680nm) for visible light-based device application. The fall of transmission below the fundamental absorption edge is steeper for the annealed films as compared to the as-prepared films presumably because of absorption due to band-to-band transition [38]. The improved crystallinity and reduced defects in the film might be the reason for this.

The absorption coefficient (α) of the prepared thin films were obtained using the equation, $\alpha = (1/t) \ln(1/T)$, Here t denotes the thickness and T indicates the transmittance of the film [39]. The absorption coefficient of the SnS films above the fundamental absorption edge were obtained in the order of 10^4 cm^{-1}. The direct optical band gap (E_g) was estimated from the $(\alpha h\nu)^2$ versus photon energy ($h\nu$) plot which is shown in Fig. 4b. The optical bandgap decreased with increase in annealing temperature reaching 1.36 eV for the film annealed at 350 °C from 1.75 eV for the as-deposited film. High optical

bandgap obtained for the as-deposited film could be due to lack of crystallinity and amorphous phase present in the film. Due to the increased crystallinity with increase in annealing temperature, optical bandgap reduced to 1.72 eV, 1.66 eV, 1.53 eV and 1.45 eV for the films annealed at 150 °C, 200 °C, 250 °C and 300 °C respectively. Reduction in optical bandgap with increase in annealing temperature is in consistent with the reported values [40].

The red-shift of the transmittance can lead to the decrease of bandgap due to minimum lattice strain with nanocrystalline behavior. Presence of other impurity phases, SnS$_2$ and Sn$_2$S$_3$ could be the reason for observed high bandgap in the film annealed at 200 °C (1.66 eV) and 250 °C (1.53 eV). The 300 °C annealed SnS film has low bandgap which can absorb more visible light than other films. Consequently, the performance of photodetector can be improved due to the higher photo-electric interaction in the semiconducting SnS film. Moreover, the presence of impurity phase of SnS$_2$ and Sn$_2$S$_3$ can also lead to improve the photocurrent value with respect to applied voltage.

3.4 Photodetector characteristics

The photodetector was fabricated by depositing Ag contacts on SnS thin films using a metal mask and the photo-response was tested under dark and 532 nm illumination condition with different power intensities. Figure 5 illustrates the detectors current–voltage (I–V) characteristics in the dark and with illumination. To clearly distinguish the photocurrent from dark current, the I–V curves are shown on a semi-log
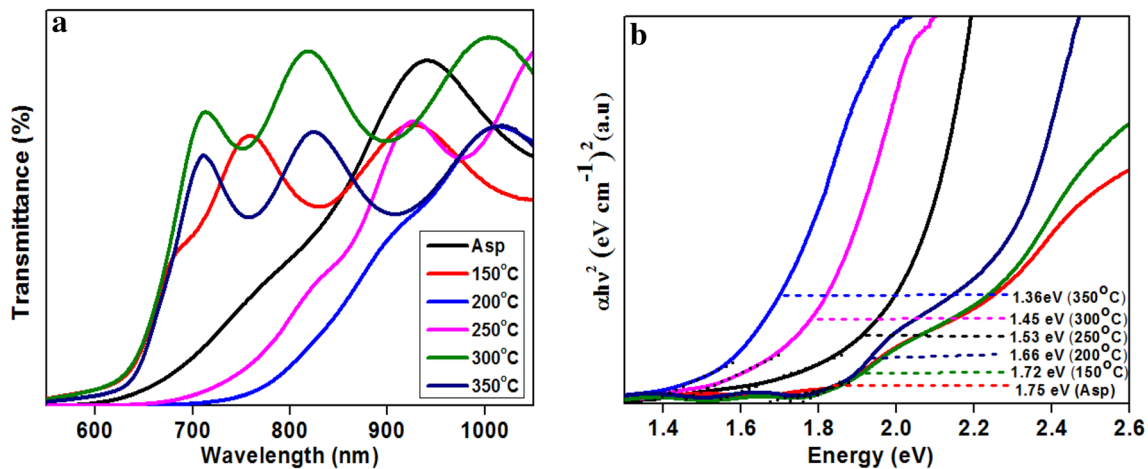
Fig. 4 **a** Optical transmittance spectra, **b** $(\alpha h\nu)^2$ versus photon energy ($h\nu$) plot of as-deposited and annealed SnS thin films

Fig. 5 I–V characteristics of the fabricated SnS thin film photodetectors under dark and illumination
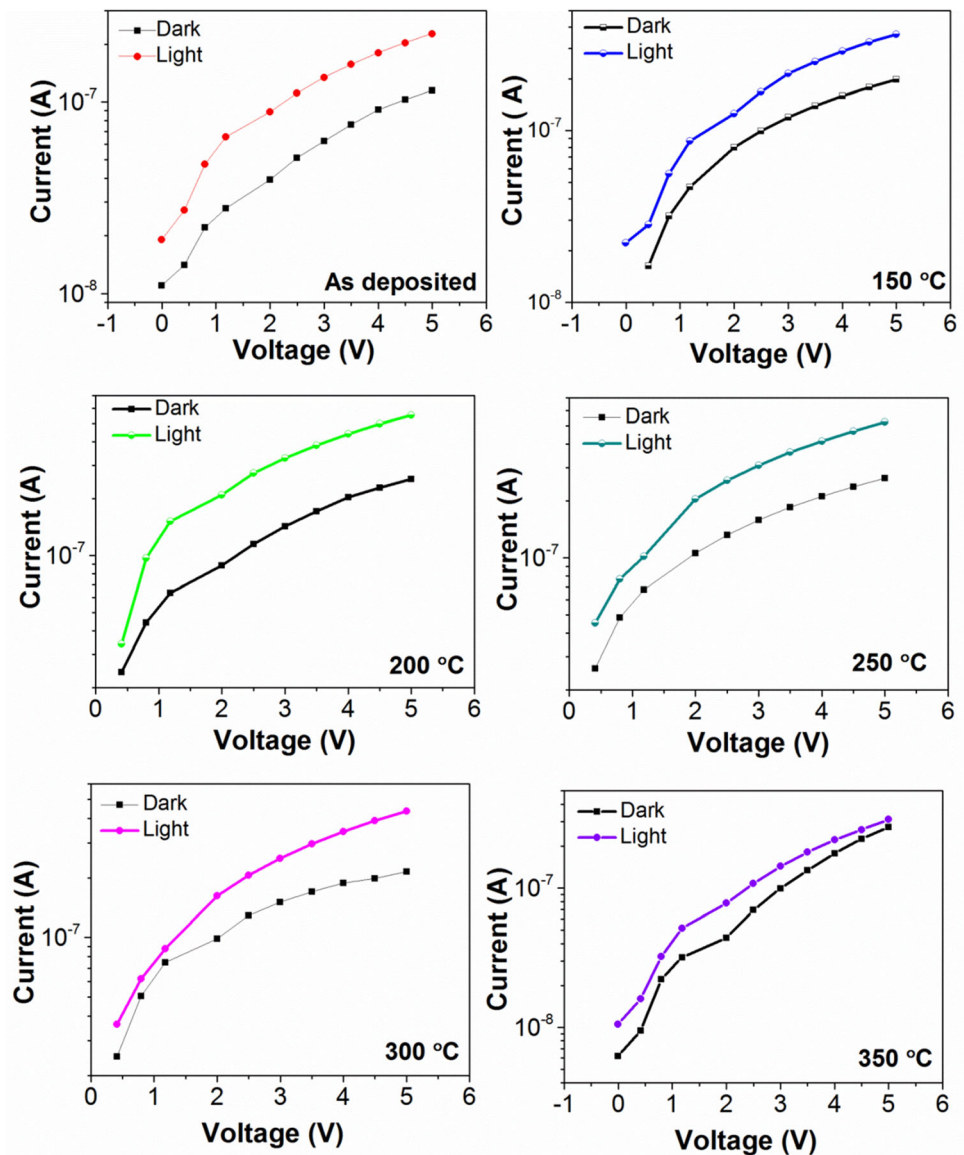
scale. The current increases linearly with the increase in bias voltage, demonstrating that the Ag electrodes and the SnS layer has an ohmic contact.

The dark current is $\sim 2 \times 10^{-7}$ A at 10 V bias for the as-deposited thin film and is gradually increased to 5×10^{-7} A for the film annealed at 300 °C. The film annealed at 350 °C showed very high dark current of $\sim 1 \times 10^{-6}$ A at 10 V bias which can be attributed to the formation of SnS_2 impurity phase and consequent increase of ionized Sn^{2+} vacancies.

Tin sulphide is intrinsically a p-type semiconductor, and its p-type conductivity is due to ionised tin vacancies (Sn^{2+}) [41]. Reddy et al. [22] discovered that sulfurized SnS thin films contain Sn in the + 2 oxidation state. With increasing annealing

temperature, this rise in ionized Sn vacancies can result in an increase in the conductivity of the films. This is also substantiated by a significant rise in the concentration of p-type carriers from 10^{15} to 10^{16} cm^3 during vacuum annealing at 300 °C [35]. Due to the fact that dark current is finite, it contributes to noise power, decreasing the signal to noise ratio.

The rise in current (or photocurrent) in the presence of light is attributable to the activation of electron–hole pairs in the SnS layer. The photocurrent (I_{PC}) is determined using $I_{PC} = I_{light} - I_{dark}$, where, I_{light} is the current when illuminated by light of wavelength 532 nm at the power density of 5 mW cm^{-2}. A photocurrent of 3×10^{-7} A was observed at 10 V bias for as-deposited thin film and is increased

with annealing temperature reaches to 6×10^{-7} A for the film annealed at 200 °C. The photocurrent drastically decreased beyond 250 °C and reaches to the value of dark current for the film annealed at 350 °C. The appearance of SnS_2 impurity phase in SnS would limit the photodetector performance due to the presence of Sn^{4+} which form acceptor impurity state and act as electron trap state. The increase in photocurrent with increasing annealing temperature up to 250 °C is ascribed to the SnS films increased crystallinity and decreased defect density.

Figure 6 depicts time dependent photo-response of fabricated SnS thin films at varying power density from 1 to 5 mW/cm² for 5 V bias. It can be seen from the figure that the response in the current value of the fabricated device was scaled linearly with respect to the incident light power except the sample annealed at 350 °C. Within the range of recorded light intensities, no photocurrent saturation occurs. The rise and fall times (τ_r and τ_f) of a photodetector are two critical characteristics for determining its response speed.

The response time 'τ_r' is normally defined as "the time interval required for the response to rise from 10 to 90% of its maximum value" whereas the recovery time 'τ_d' is "the time interval for the response to decay from 90 to 10% of its peak value". The estimated rise time and fall time for the film annealed at 200 °C (see Fig. 7) was found to be 4.8 s and 5.2 s, respectively.

Fig. 6 Photocurrent variations of the SnS detectors measured under 532 nm with different light intensity from 1 to 5 mW/cm²
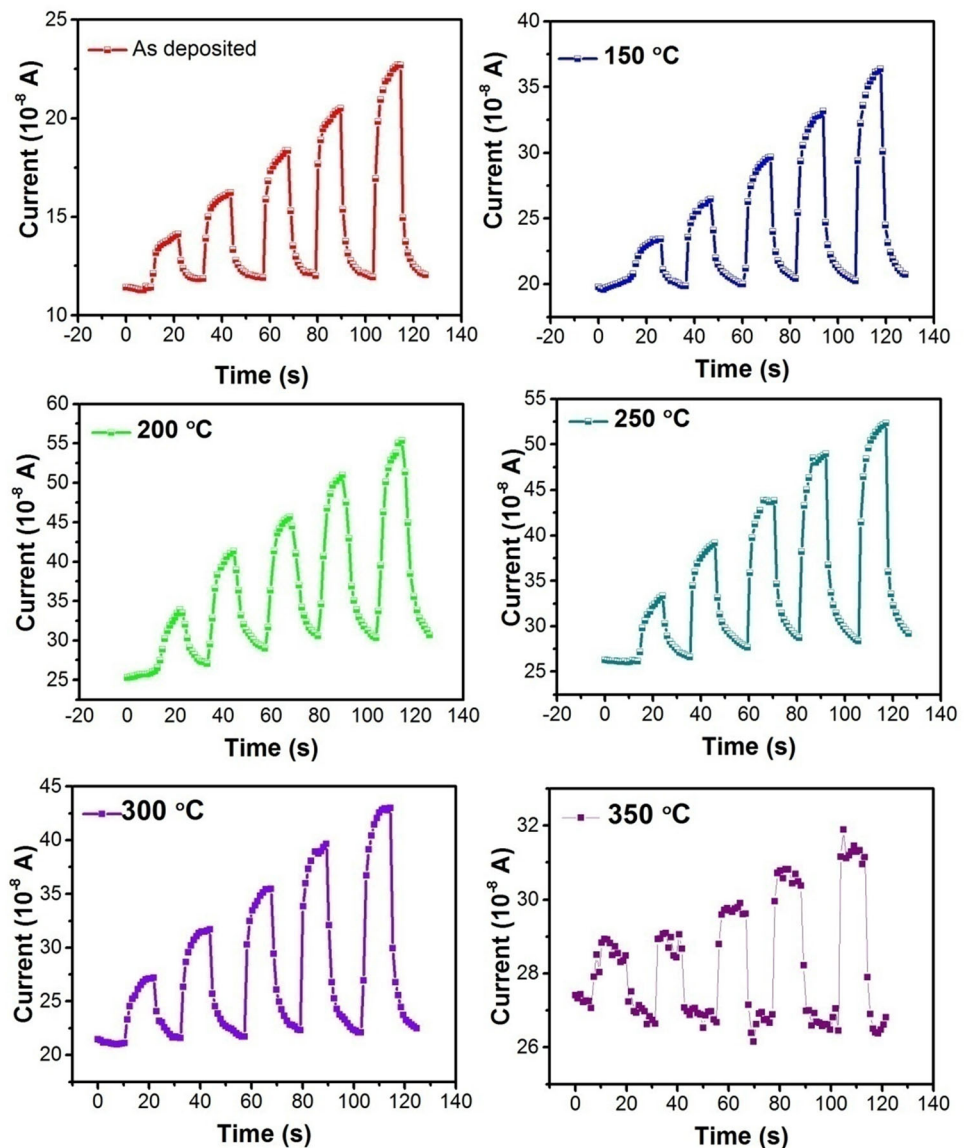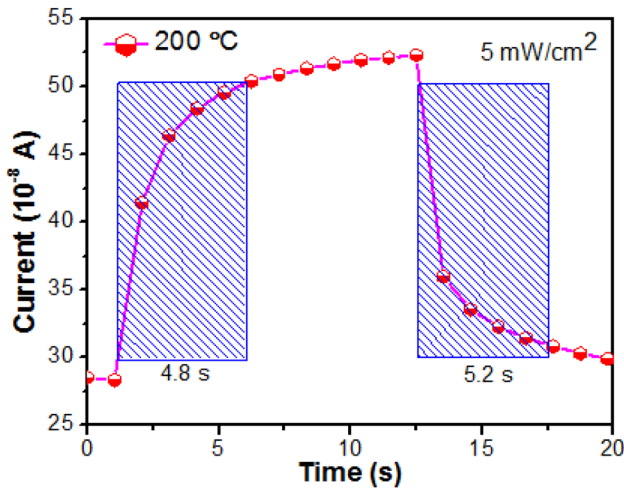
**Fig. 7** Response and recovery time of SnS thin film annealed at 200 °C

3.5 Photosensing parameters (R), (D*) and (EQE)

The (R), (EQE), and (D*) are the three important parameters for evaluating the performance of the photo detectors. The photo responsivity (R) i.e., "the amount of photocurrent generated per unit area per unit illumination intensity" is determined by the ratio of photocurrent value (I_{PC}) to the incident power density (P_{in}) by the relation below $= I_{PC}/A \cdot P_{in}$, where A is the active area of the detector. Detectivity, D* and EQE can be estimated from R value as following by the relation $D^* = RA^{1/2}/2eI_{dc}$, while, EQE is estimated using the relation $EQE = Rhc/[39]$, where h,c, e, are constant with usual meaning and λ is the wavelength of the illuminating laser source used.

Figure 8 shows the Responsivity (R), specific detectivity (D*) and external quantum efficiency (EQE) of the films annealed at the temperature range of 150 °C to 350 °C. It is clear from the figure that all these photodetector parameters reached maximum value for the film annealed at 200 °C and decreases with further increase in annealing temperature.

The responsivity of the detector swiftly increases from 0.03 to 0.06 AW^{-1} when the annealing temperature increased from 15 to 200 °C. Reddy et al. [25] reported the maximum responsivity of 0.43×10^{-3} AW^{-1} for the SnS detector under visible light which is lower than our value. The fabricated device has the highest responsivity of 0.06 AW^{-1}, a maximum EQE of 14%, and the highest detectivity of 6.8×10^{10} jones for the film annealed at 200 °C. This is due to the maximum ratio of both dark and photocurrent observed in the prepared SnS detector. It is worth noting that the detectivity obtained in the present study is nearly two orders higher than the previous report ($D^* = 7.1 \times 10^7$ Jones) [25] for SnS visible photo detector.

There are several mechanisms which can be explained for the performance of photodetector under light illumination. But the main process is for generating electron–hole pairs with respect to light power density. Usually, the electron–hole pair is generated via optical absorption when the illumination energy is higher than the bandgap energy of the absorbing material which is known as above band energy illumination [22]. Here, the band gap of the SnS films is around 1.75 eV–1.36 eV which are quite lower than the illuminated light energy is about
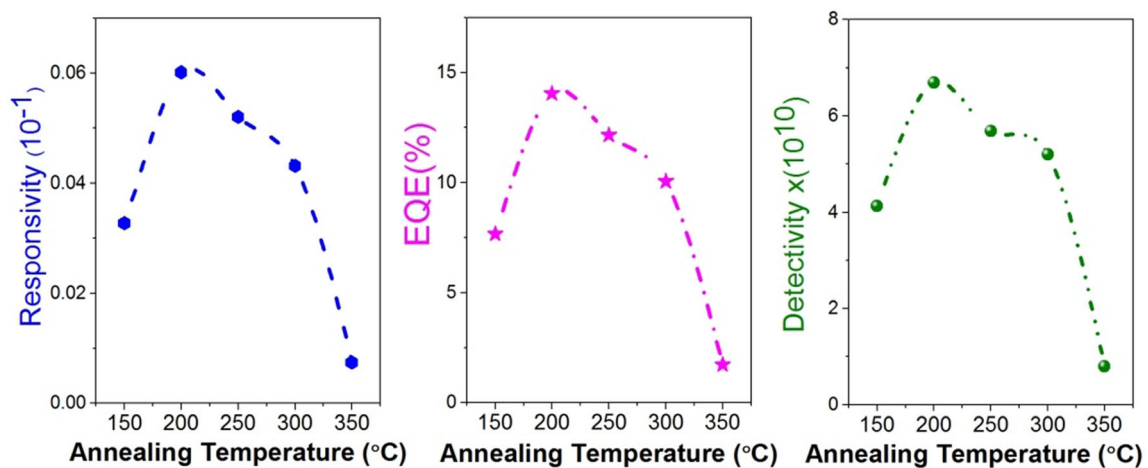
Fig. 8 The variations of responsivity (R), specific detectivity (D*) and EQE with respect to different annealing temperature.

2.33 eV (532 nm), therefore, above band energy illumination is occurring to generate the electron–hole pairs. Consequently, there is an increase of photocurrent when compared to the dark current. In addition to that the observed impurity phase of Sn_2S_3 (at 200 °C) could also help to enhance the photocurrent by the vacancy of Sn^{2+} ions.

4 Conclusions

Tin sulfide (SnS) thin films were developed using thermal evaporation technique on glass substrate and were annealed in N_2 atmosphere for 2 h in a temperature range of 150 °C–350 °C in order optimize their physical properties for visible light photodetector application. The annealed films retain its stoichiometry up to 300 °C beyond which films will be sulfur deficient. The degree of crystallinity increased with annealing temperature as reveled by XRD analysis. Raman analysis confirmed the formation of pure SnS phase in as-deposited film; while impurity phase of SnS_2 was present in the film annealed at 350 °C. The fall of transmission below the fundamental absorption edge is steeper for the films annealed at temperatures > 200 °C mainly absorption due to direct band-to-band transition. The photo response of the fabricated photodetectors was tested under dark and illumination condition by using 532 nm laser. A gradual increase of photocurrent from as-deposited to annealed SnS films and reaches maximum for 200 °C. The rise time and decay time estimated for the film annealed at 200 °C was found to be 4.8 s and 5.2 s respectively. The device fabricated had the highest Responsivity of 0.06 AW^{-1}, a maximum EQE of 14%, and the highest detectivity of 6.8×10^{10} jones for the film annealed at 200 °C. Thus, good stability, high responsivity and fast response time of the photodetectors based on thermally evaporated and subsequently annealed SnS thin films in N_2 atmosphere make it an appealing material for visible light photodetector application.

Author contributions

DA: original draft, Software, Data curation, Investigation. SSH: Visualization, Experiments. SV: Experiments. KDAK: Visualization, Experiments. RN: Visualization, Methodology, Experiments. SPP: Experiments. MEESM: Experiments. RG: Conceptualization, Methodology, Writing—review & editing, Supervision.

Data availability

The data that support the findings of this study are available from the corresponding author upon reasonable request.

Declarations

Conflict of interest The authors declare that they have no conflicts of interest.

Ethical approval This article does noy contain any studies involving animals performed by any of the authors. Also, this article does not contain any studies involving human participants performed by any of the authors.

References

1. D. Wang, H. Wu, Y. Xiao, Y. Zhang, D. He et al., High thermoelectric performance in low cost $SnS_{0.91}Se_{0.09}$ crystals. Science **365**, 1418–1424 (2019)
2. S. Varadharajaperumal, D. Alagarasan, C. Sripan, R. Ganesan, M.N. Satyanarayan, G. Hegde, Toxic-free surface level sulphur doped 1D Ti-Ox-Sy nanorods for superstrate heterojunction CZTS thin-film solar cells. Mater. Res. Bull. **133**, 111081 (2021)
3. S.S. Hegde, B.S. Surendra, V. Talapatadur, M. Prashanth, K. Ramesh, Visible light photo T = $4A_g + 2B_{1g} + 4B_{2g} + 2B_{3g} + 2A_u + 4B_{1u} + 2B_{2u} + 4B_{3u}$ catalytic properties of cubic and orthorhombic SnS nanoparticles Chem. Phys. Lett. **54**, 137665 (2020)

4. Y. Huang, H.X. Deng, K. Xu, Z.X. Wang, Q.S. Wang, F.M. Wang, F. Wang, X.Y. Zhan, S.S. Li, J.W. Luo, J. He, Highly sensitive and fast phototransistor based on large size CVD-grown SnS_2 nanosheets. Nanoscale **7**, 14093–14099 (2015)

5. H. Dittrich, A. Stadler, D. Topa, H.J. Schimper, A. Basch, Progress in sulfosalt research. Phys. Status Solidi A **206**, 1034–1041 (2009)

6. K.D. Arun Kumar, P. Mele, M. Anitha, S. Varadharajaperumal, D. Alagarasan, N.S. Alhokbany, T. Ahamad, S.M. Alshehri, Simplified chemical processed Cd_{1-x} Al $_x$ S thin films for high-performance photodetector applications. J. Phys. Condens. Matter. **33**, 195901 (2021)

7. D.A. Nguyen, H.M. Oh, N.T. Duong, S. Bang, S.J. Yoon, M.S. Jeong, Highly enhanced photoresponsivity of a monolayer WSe_2 photodetector with nitrogen-doped graphene quantum dots. ACS Appl. Mater. Interfaces **10**, 10322–10329 (2018)

8. L.A. Burton, D. Colombara, R.D. Abellon, F.C. Grozema, L.M. Peter, T.J. Savenije, G. Dennler, A. Walsh, Synthesis, characterization, and electronic structure of single-crystal SnS, Sn_2S_3, and SnS_2. Chem. Mater **25**, 4908–4916 (2013)

9. S.H. Kwon, B.H. Kim, D.W. Kim, H. Yoon, Y.J. Yoon, Vastly enhanced photo responsivities of phase-controlled tin sulfide thin films. Nanotechnology **31**, 375702 (2020)

10. V. Steinmann, R. Jaramillo, K. Hartman, R. Chakraborty, R.E. Brandt, J.R. Poindexter, Y.S. Lee, L. Sun, A. Polizzotti, H.H. Park, R.G. Gordon, T. Buonassisi, 3.88% efficient tin sulfide solar cells using congruent thermal evaporation. Adv. Mater. **26**, 7488–7492 (2014)

11. J.B. Johnson, H. Jones, B.S. Latham, J.D. Parker, R.D. Engelken, C. Barber, Optimization of photoconductivity in vacuum-evaporated tin sulfide thin films. Semicond. Sci. Technol. **14**, 501 (1999)

12. C. Schreyvogel, S. Temgoua, C. Giese, V. Cimalla, J. Barjon, C.E. Nebel, Fabrication of n-type doped V-shaped structures on (100) Diamond. Phys. Status Solidi A **218**, 2000642 (2021)

13. Y. Shan, Y.L.H. Pang, Applications of tin sulfide-based materials in lithium-ion batteries and sodium-ion batteries. Adv. Funct. Mater. **30**, 2001298 (2020)

14. S. Gedi, V.R.M. Reddy, T.R.R. Kotte, S.H. Kim, C.W. Jeon, Chemically synthesized Ag- doped SnS films for PV applications, javascript:void(0). Ceram. Int. **42**, 19027–19035 (2016)

15. P. Sinsermsuksakul, L. Sun, S.W. Lee, H.H. Park, S.B. Kim, C. Yang, R.G. Gordon, Overcoming efficiency limitations of SnS-based solar cells. Adv. Energy Mater **1400496**, 1–7 (2014)

16. A. Javed, N. Khan, S. Bashir, M. Ahmad, M. Bashir, Thickness dependent structural, electrical and optical properties of cubic SnS thin films. Mater. Chem. Phys. **246**, 122831 (2020)

17. M. Haghighi, M. Minbashi, N. Taghavinia, D.H. Kim, S.M. Mahdavi, A.A. Kordbacheh, A modelling study on utilizing SnS_2 as the buffer layer of CZT(S, Se) solar cells. Sol. Energy **167**, 165–171 (2018)

18. S. Ullah, A. Bouich, H. Ullah, B. Mari, M. Molars, Comparative study of binary cadmium sulfide (CdS) and tin disulfide (SnS2) thin buffer layers. Sol. Energy **208**, 637–642 (2020)

19. Y. Xu, N.A. Salim, C.W. Bumby, R.D. Tilley, Synthesis of SnS quantum dots. J. am. Chem. Soc **131**, 15990–15991 (2009)

20. S.S. Hegde, A.G. Kunjomana, K.A. Chandrasekharan, K. Ramesh, M. Prashantha, Optical and electrical properties of SnS semiconductor crystals grown by physical vapor deposition technique. Phys. B Condens. Matter **406**, 1143–1148 (2011)

21. S.S. Hegde, M. Prashantha, B.J. Fernandes, R. Venkatesh, K. Ramesh, Synthesis, thermal stability and structural transition of cubic SnS nanoparticles. J. Alloys Comp. **820**, 153116 (2020)

22. V.R.M. Reddy, S. Gedi, C. Park, R.W. Miles, Development of sulphurized SnS thin film solar cell. Curr. Appl. Phys. **15**, 588–598 (2015)

23. P. Sinsermsuksakul, L. Sun, S.W. Lee, H.H. Park, S.B. Kim, C. Yang, R.G. Gordon, Atomic layer deposition of tin monosulfide thin films. Adv. Energy Mater. **4**, 1400496 (2014)

24. S. Yuan, G. Liu, H. Tian, C. Fan, M. Wang, E. Li, Facile synthesis of tin monosulfide nanosheets via physical vapour deposition and their near-infrared photoresponse. AIP Adv. **9**, 095205 (2019)

25. T.S. Reddy, M.C. Santhosh Kumar, Co-evaporated SnS thin films for visible light photodetector applications. RSC Adv. **6**, 95680 (2016)

26. M.S. Mahdi, K. Ibrahim, A. Hmood, N.M. Ahmed, S.A. Azzez, F.I. Mustafa, A highly sensitive flexible SnS thin film photodetector in the ultraviolet to near infrared prepared by chemical bath deposition. RSC Adv. **6**, 114980 (2016)

27. G. Liu, Y. Li, B. Li, H. Tian, C. Fan, Y. Zhang, Z. Hua, M. Wang, H. Zheng, E. Li, Visible phototransistors based on vertical nanolayered heterostructures of SnS/SnS2 p–n and SnSe2/SnS2 n–n nanoflakes. J. Mater. Chem. C **00**, 1–3 (2018)

28. V.P. Jethwaa, K. Patel, N. Som, V.M. Pathak, K.D. Patel, G.K. Solanki, P.K. Jha, Temperature dependent vibrational properties of DVT grown orthorhombic SnS single crystals and their applications as a self-powered photodetector. Appl. Surf. Sci. **531**, 147406 (2020)

29. G.M. Kumar, X. Fu, P. Ilanchezhiyan, S.U. Yuldashev, D.J. Lee, H.D. Cho, T.W. Kang, Highly sensitive flexible photodetectors based on self-assembled tin monosulfide nanoflakes with graphene electrodes. ACS Appl. Mater. Interfaces **9**, 32142–32150 (2017)

30. X. Zhou, L. Gan, Q. Zhang, X. Xiong, H. Li, Z. Zhong, J. Han, T. Zhai, High performance near-infrared photodetectors based on ultrathin SnS nanobelts grown via physical vapor deposition. J. Mater. Chem. C **2016**, 1–10 (2016)

31. M.S. Mahdi, K. Ibrahim, N.M. Ahmed, A. Hmood, S.A. Azzez, Growth and characterization of tin sulphide nanostructured thin film by chemical bath deposition for near-infrared photodetector. Appl. Solid State Phenom. **290**, 220–224 (2019)

32. M.S. Mahdi, K. Ibrahim, N.M. Ahmed, A. Hmood, F.I. Mustafa, S.A. Azzez, M. Bououdina, High performance and low-cost UV-Visible-NIR photodetector based on tin sulphide nanostructures. J. Alloys Comp. **735**, 2256–2262 (2018)

33. F. Lu, J. Yang, R. Li, N. Huo, Y. Li, Z. Wei, J. Li, Gas-dependent photoresponse of SnS nanoparticles-based photodetector. J. Mater. Chem. C **3**, 1397–1402 (2015)

34. S.S. Hegde, A.G. Kunjomana, K. Ramesh, K.A. Chandrasekharan, M. Prashantha, Preparation and characterization of SnS thin films for solar cell application Inter. J. Soft Comp. Eng. (IJSCE) **1**, 38–40 (2011)

35. S.S. Hegde, A.G. Kunjomana, P. Murahari, B.K. Prasad, K. Ramesh, Vacuum annealed tin sulfide (SnS) thin films for solar cell applications. Surf. Interfaces **10**, 78–84 (2018)

36. P. Jain, P. Arun, Influence of grain size on the band-gap of annealed SnS thin films. Thin Solid Films **548**, 241–246 (2013)

37. R. Naik, P.P. Sahoo, C. Sripan, R. Ganesan, Laser induced Bi diffusion in As40S60 thin films and the optical properties change probed by FTIR and XPS. Opt. Mater. **62**, 211–218 (2016)

38. D. Sahoo, P. Priyadarshini, R. Dandela, D. Alagarasan, R. Ganesan, S. Vardharajperumal, R. Naik, Optimization of linear and nonlinear optical parameters in As40Se60 film by annealing at different temperature. Optik **219**, 165286 (2020)

39. M. Behera, N.C. Mishra, R. Naik, C. Sripan, R. Ganesan, Thermal annealing induced structural, optical and electrical properties change in $As_{40}Se_{60-x}Bi_x$ chalcogenide thin films. AIP Adv. **9**, 095065 (2019)

40. J. Xu, Y. Yang, Z. Xie, Effect of vacuum annealing on the properties of sputtered SnS thin films. Chalcogenide Lett. **11**, 485–491 (2014)

41. T. Gotoh, Control of carrier concentration in SnS films by annealing with S and Sn. Phys. Status Solidi A **213**, 1869–1872 (2016)